



Article

Tectonic Significances of the Geomorphic Evolution in the Southern Alashan Block to the Outward Expansion of the Northeastern Tibetan Plateau

Tingting Ji ^{1,2} , Wenjun Zheng ^{1,2,*}, Jingjun Yang ^{1,2}, Dongli Zhang ^{1,2}, Shumin Liang ^{1,2}, Yige Li ^{1,2}, Ting Liu ^{1,2}, Haoyu Zhou ^{1,2} and Changhuan Feng ^{1,2}

¹ Guangdong Provincial Key Laboratory of Geodynamics and Geohazards, School of Earth Sciences and Engineering, Sun Yat-sen University, Guangzhou 510275, China

² Southern Marine Science and Engineering Guangdong Laboratory (Zhuhai), Zhuhai 519082, China

* Correspondence: zhengwenjun@mail.sysu.edu.cn

Abstract: Fluvial landscapes are a result of lithospheric tectonic movement, climate evolution and surface processes. Existing evidence proves that regional tectonic deformation can be reflected by the evolution of fluvial landforms. The southern Alashan Block lies the closest to the northeastern Tibetan Plateau and has become the latest plateau outward expansion boundary. Yabrai Shan is located at the intersection of the Tibetan Plateau, Alashan and Ordos Blocks, thereby recording the evolution of the surface processes and tectonic activities in the northeastern Tibetan Plateau and its surrounding regions. Herein, we conducted the quantitative landform analysis and field investigations of Yabrai Shan, and the spatiotemporal distribution of geomorphological parameters indicated that Yabrai Shan is in the mature stage of geomorphological evolution controlled by tectonic activities of the Yabrai range-front fault. Based on the paleochannel reconstruction model and previous research on fault activity, two tectonic acceleration events were identified, with estimated geomorphic response times of 0.15–1.10 Ma and 1.42–2.92 Ma. Different distribution characteristics of two-phase knickpoints are caused by the change of tectonic stress in this region, revealing that the late knickpoints are the result of tectonic acceleration under the influence of the northeast expansion of the Tibetan Plateau. The transformation of Yabrai Shan from the original extensional environment affected by the Ordos Block to the compressional environment affected by the northeast expansion of the Tibetan Plateau occurred after 1.10 Ma.

Keywords: southern Alashan block; fluvial landforms; two-phase uplift of Yabrai Shan; outward expansion of Tibetan Plateau; Late Cenozoic



Citation: Ji, T.; Zheng, W.; Yang, J.; Zhang, D.; Liang, S.; Li, Y.; Liu, T.; Zhou, H.; Feng, C. Tectonic Significances of the Geomorphic Evolution in the Southern Alashan Block to the Outward Expansion of the Northeastern Tibetan Plateau. *Remote Sens.* **2022**, *14*, 6269. <https://doi.org/10.3390/rs14246269>

Academic Editor: David Gomez-Ortiz

Received: 16 November 2022

Accepted: 7 December 2022

Published: 10 December 2022

Publisher's Note: MDPI stays neutral with regard to jurisdictional claims in published maps and institutional affiliations.



Copyright: © 2022 by the authors. Licensee MDPI, Basel, Switzerland. This article is an open access article distributed under the terms and conditions of the Creative Commons Attribution (CC BY) license (<https://creativecommons.org/licenses/by/4.0/>).

1. Introduction

The tectonic transformation between the Tibetan Plateau and Alashan Block is an important scientific topic related to the uplift and expansion of the northeastern Tibetan Plateau during the Late Cenozoic. There are numerous debates regarding this scientific topic, the majority of which focus on two issues. The first issue concerns the eastward propagation of the Altyn Tagh Fault (ATF), i.e., the ATF extending eastward and entering the interior of the Alashan Block or terminating at the western end of the Hexi Corridor, which is related to the two major hypotheses regarding the northern Tibetan Plateau deformation [1–6]. The second issue concerns the north-eastward expansion pattern of the Tibetan Plateau, i.e., the stepwise northeastern expansion or its quasi-contemporaneous deformation at the northeastern margin. The Tibetan Plateau gradually extended to the Alashan Block through tectonic transformation [7–9]. However, adequately addressing these issues requires extensive research in a variety of areas, such as active tectonics and the Late Cenozoic tectonic deformation. The southern Alashan Block lies the closest to the northeastern Tibetan Plateau and has become the latest plateau outward expansion

boundary [10]. Yabrai Shan is located at the intersection of the Tibetan Plateau, Alashan and Ordos Blocks, recording the surface processes and tectonic activities around the surrounding regions. Previous studies in this area have focused on the Mesozoic-Cenozoic tectonic evolution of the basins and mountains [5,11,12] and the Late Quaternary slip-rate of the Yabrai range-front fault [13–15]. Clarifying the relevant content is of great significance in order to comprehend the tectonic transformation between the northeastern margin of the Tibetan Plateau and southern Alashan Block.

Fluvial landforms record signs of fault activity, depositional processes and incisions. Accelerations of mountain uplifts are attributed to the tectonic activities of the controlling faults [16–18]. Bedrock channels adjust the slope of the channels to enhance the incision rates and achieve new equilibrium states [16], and the adjustments of stream longitudinal profiles are achieved through knickpoint migrations [17]. Previous research has highlighted quantitative analysis of fluvial landforms and provides a practical approach for interpreting the interactions between tectonic activities and surface processes [18]. The stream power model and related geomorphic parameters, based on numerous field investigations and numerical simulations, are used for depicting the spatiotemporal patterns of tectonic activities in active orogenic belts [19–22]. The stream power model and relevant sub-models have been widely used in quantitative analyses of fluvial landscapes, such as the eastern [21] and northeastern margins of the Tibetan Plateau [22], and the Andes in South America [23].

In this study, we obtained a series of geomorphological parameters and conducted a field investigation to assess the fluvial evolution of Yabrai Shan. By conducting the quantitative geomorphological analysis based on the ASTER GDEM 30 m data and surveying the distribution of geomorphological parameters, we study the relationship of terrain-geomorphic parameters-tectonic activities, discuss the implication of knickpoints and estimate the geomorphic response time.

2. Geological Setting

Yabrai Shan is located at the intersection of the Tibetan Plateau, Alashan and Ordos Blocks; it is an important mountain range in the southern Alashan Block and the natural boundary between the Badain Jaran and Tengger Deserts (Figure 1a). The Yabrai range-front fault is approximately 80 km long, lies at the boundary between the Yabrai Shan and Yabrai Basin and is an important active fault in the Alashan Block [3,23]. It exhibits a normal fault, with low slip rate and less modern, strong earthquakes [24,25].

According to the difference of fault strike and geomorphology features, the fault can be divided into three segments, namely the southwest, middle, and northeast segments (Figure 1b). The southwest segment strikes 60°NE and extends approximately 35 km along the front of Yabrai Shan; it is dominated by normal fault activity, accompanied by left-lateral-slip motion and cuts off the root of the alluvial fan near the foot of the mountain. The middle segment is approximately 30 km long and strikes 40°NE; its typical geomorphological feature is the fault bedrock surfaces formed by normal faults, and faults migrate towards the basin. The northeast segment strikes 75°N–85°E, and it is dominated by left-lateral-slip motion with thrust components [11].

The strata in the Yabrai Shan are primarily Cenozoic, Mesozoic and Precambrian, while there is also a small number of Paleozoic deposits. The Precambrian strata are the oldest crystalline basement in this region. It is a set of shallow to medium-deep metamorphic rocks with complex lithology and huge thickness, mainly composed of schist, gneiss and migmatite, scattered in the magmatic rocks. The Paleozoic strata are practically undeveloped, with few exposed Carboniferous-Permian strata. The Mesozoic strata are primarily Jurassic and Cretaceous. The Jurassic strata is a set of continental sedimentary clastic rocks with complex clastic compositions, indicating the depositional environment of fluvial and lacustrine facies. The Cretaceous strata is a set of variegated clastic deposits, indicating an alternating depositional environment of lacustrine and alluvial facies. Except for bedrock mountains, most of the areas are Cenozoic alluvial and

aeolian deposits. Magmatic rocks developed in this region, including Mesoproterozoic, Paleozoic and Mesozoic. The rocks are influenced by their regional structure, striking NE–SW, and the foliation and gneissosity are mostly oriented in the same direction. The main lithology is granite, diorite and gabbro [26].

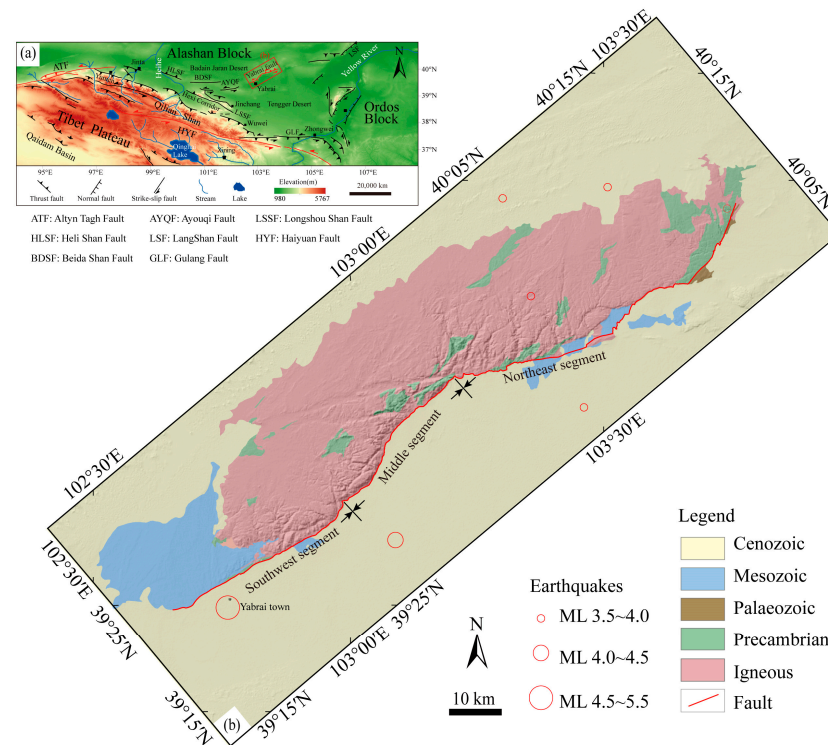


Figure 1. (a) Topography and major active faults in the northeast Tibetan Plateau, modified from [6,12]. (b) The geological map of Yabrai Shan. The red box in (a) shows the location of Yabrai Shan. The red line and red circles in (b) represent the Yabrai range-front fault and seismicity in this area. Fault data from [12,26] and seismicity data from CENC and USGS catalogue.

Yabrai Shan is characterized by a dry continental climate with cold and dry winters, hot and dry summers and an average temperature of 9.6 °C. It is dry all year with little rainfall and snowfall, and high evaporation, with the annual average evaporation being 30 times greater than the average annual precipitation. Water resources are scarce, comprising primarily seasonal rivers. Most of the surface water is temporary with strong seasonality, primarily accumulating towards the basin after heavy rainfall. The rivers in this region are usually dry, and ice and snow meltwaters are not present, nor are flowing tributaries. Flowing water occurs only during heavy rainfall in the summer, and its flow is dependent on the amount of precipitation [26].

3. Methods

3.1. Stream Power Incision Model

The stream power incision model considers the channel elevation change as the difference between the bedrock uplift rate and the stream erosion rate. When the bedrock uplift is balanced with the river erosion, the channel elevation no longer changes, and the channel morphology tends to be stable. For a channel in a steady state, a channel profile analysis can be performed. The erosion rate of the bedrock channel is primarily determined by the erosive capacity of the river. Erosion rate E is expressed as a function of the erosion coefficient, drainage area and channel slope [16,27,28]:

$$E = KA^m S^n \quad (1)$$

where K is the erosion coefficient affecting the relationship between the erosion rate, watershed area and channel gradient, including the effects of climate, lithology, sedimentary flux and channel width on the erosive capacity of the river. A is the drainage area, S is the channel slope, m is the drainage area index and n is the channel gradient index; both m and n are positive indices.

According to the stream power incision model, the change of river channel elevation depends on the difference between the bedrock uplift and river erosion rates, and can be expressed as follows:

$$\partial z / \partial t = U(x, t) - KA^m (\partial z / \partial x)^n \quad (2)$$

where z is the channel elevation, x is the distance from the bedrock channel to the outlet, t is time and U is the rock uplift rate. When the river reaches equilibrium, the bedrock uplift rate is equal to the river incision rate, the elevation of the river no longer changes and the channel profile remains stable. Subsequently, Equation (2) can be written as follows:

$$0 = U - KA^m (dz/dx)^n \quad (3)$$

Equation (3) can also be expressed as follows:

$$S = (U/K)^{1/n} A^{-m/n} \quad (4)$$

Equation (4) is obtained through physical derivation, and its form is consistent with the empirical model based on actual observations [16,28]. According to the empirical model, the channel gradient is a power function of the drainage area.

$$S = k_s A^{-\theta} \quad (5)$$

where k_s and θ are two important geomorphological parameters that express channel profile characteristics [28]:

$$k_s = (U/K)^{1/n} \quad (6)$$

$$\theta = m/n \quad (7)$$

Here, k_s is the channel steepness index, which is a function of the uplift rate U and erosion rate K , and indicates the difference in regional uplift activity [22,27,29–32]. θ is the channel concavity and indicates the depression degree in the channel. In general, θ ranges between 0.3 and 0.6; it is not significantly affected by the structure and is related to lithology, climate and erosion processes [17,18,20].

The log-log slope-area method is the conventional approach regarding channel profile analysis; it linearly regresses the log value of the slope and drainage area, with the negative of slope being concavity and the intercept being the log value of the steepness index. However, the calculation of slope requires a series of operations such as smoothing, resampling and differentiation of elevation, thereby introducing problems, such as large deviation of the regression analysis error results [31]. To address this, an integration approach was developed. It directly solves the steady-state stream power incision equation and yields the analytical formula for the channel elevation z as a continuous function, thereby avoiding the deviation caused by calculating the slope. Equation (3) can also be expressed as follows:

$$dz = (U/K)^{1/n} A^{-m/n} dx \quad (8)$$

Both sides of Equation (8) are integrated as follows:

$$z = (U/K)^{1/n} \int_{x_b}^x (A_0/A(x'))^{m/n} dx' + z(x_b) \quad (9)$$

where $z(x_b)$ is the elevation of the water outlet. To ensure that the dimensions of the integral term were the same as those of the traceability distance of the channel, A_0 was introduced as a reference drainage area.

Here, χ was introduced and constrained by the topological information of the river [33]:

$$\chi = \int_0^x (A_0/A(x'))^{m/n} dx' \quad (10)$$

where A_0 can be any value with a physical unit corresponding to the actual drainage area. A_0 was set to 1, and the watershed outlet was set as the boundary condition of the equation, i.e., $z(x_b) = 0$. Therefore, Equation (9) was written as follows:

$$z(x) = k_s \chi(x) \quad (11)$$

The χ -plot was drawn with the χ value as the abscissa and elevation z as the ordinate, thereby being a straight line passing through the origin, and the gradient of the χ -plot being the river steepness index. Abrupt changes of k_{sn} from upstream to downstream in the channel longitudinal profiles were recognized as knickpoints.

Knickpoints can be characterized as moving points along the bedrock channel [18]. There are two forms of knickpoints: vertical-step and slope-break (Figure 2) [34]. Both morphologies can be identified on slope-distance, slope-area or χ -plot plots, featured with obvious changes of channel gradient. Vertical-step knickpoints are spatially related to the discrete heterogeneity along the profile. The spatial correlation of landslides, debris flows or coarse gravel of locally resistant substrate at tributary junctions and tributaries depicts that these are usually fixed in space. Thus, the vertical-step knickpoint has no direct tectonic significance, except in most landslides in rapidly rising areas. Slope-break knickpoints constitute the spatiotemporal response to persistent changes. When erosion occurs, these knickpoints migrate to the upper reach at a predictable rate; while developing systematic patterns, they play a significant role in the tectonics interpretation of erosion landform.

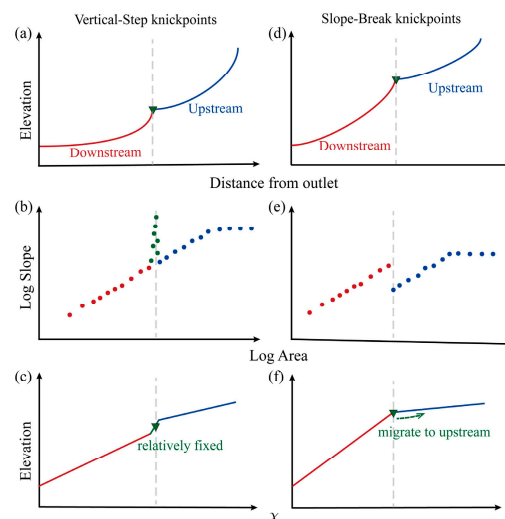


Figure 2. Classification of knickpoints in terms of (a,d) the channel profile, (b,e) log-log slope-area and (c,f) χ -plot, modified from [34]. Assuming both the upstream and downstream channels have reached the stable state, the geomorphic response time of a knickpoint can be estimated by the stream power incision mode. The blue, red lines and green points represent the upstream channel, downstream channel and knickpoints, respectively. The morphologies depict a transient perturbation of the fluvial system or fixed in place by a resistant substrate, landslide debris or active faults.

Based on the above principle, the distance between two knickpoints can be expressed as follows:

$$\Delta z = (U_1 - E)\tau \tag{12}$$

where Δz is the difference of the erosion amount, U_1 represents the uplift rate of the downstream channel, U_2 represents the uplift rate of the upstream channel and τ is the geomorphic response time, which is also the time of forming knickpoints (Figure 3).

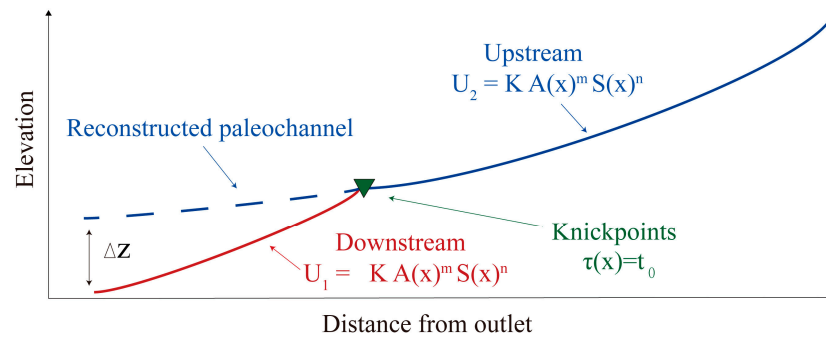


Figure 3. Schematic diagram of the paleochannel reconstruction, modified from [34].

When the exponent n equals 1, according to Equation (2), the response time of the knickpoints can be constrained by [35–37]:

$$\tau = \Delta z / (U - E) = \Delta z / U_1 [1 - k_{sn2} / k_{sn1}] \tag{13}$$

where Δz refers to the relative elevation between the knickpoint and the water outlet and k_{sn1} and k_{sn2} represent the normal steepness index of the downstream and upstream, respectively. These parameters can be obtained through river longitudinal profile analysis. U_1 is the current tectonic activity rate, which can be obtained through thermal chronological data, cosmogenic nuclides, river downcutting rate and other methods [16,30,35,36].

3.2. Hypsometric Integral

For a watershed, the ratio $z(x)/z_{max}$ of any elevation to the maximum elevation is taken as the ordinate, the ratio $A(x)/A_{max}$ of the area above elevation to the total watershed area is taken as the abscissa and the resulting graph is called a hypsometric integral curve [38]. The area enclosed by this curve and the horizontal and vertical axes are the hypsometric integrals (HI), which can be expressed as follows:

$$HI = \int_0^1 z(x)/z_{max} d[A(x)/A_{max}] \tag{14}$$

When the area is larger than 1 km², it is dominated by fluvial erosion [17,18,38]. Equations (10) and (11) can be imported into Equation (14), which can subsequently be simplified through integration by parts:

$$HI' = k_s / z_{max} \cdot 1 / A_{max} \left[\left(A(x) \int_0^x (1/A(x))^{m/n} dx' \right) \Big|_0^L + \int_0^L (1/A(x))^{m/n} \cdot A(x) dx \right] \tag{15}$$

Compared to the total area of the watershed, the drainage area in the headwaters was extremely small. The $A(L)/A_{max}$ value was approximately equal to 0. Equation (15) can be simplified as follows:

$$HI' = k_s / z_{max} \cdot 1 / A_{max} \int_0^L (1/A(x))^{m/n} \cdot A(x) dx \tag{16}$$

Equation (16) is a definite integral, and HI is proportional to the river steepness index k_s . The HI index reflects the strength of the regional tectonic activities [39,40].

4. Results

Landforms are generally shaped by tectonic movements and carved by denudation processes. Geomorphological parameters were calculated to clarify whether the feedbacks between fluvial landform evolution and regional tectonic activities are significant. In this study, based on the Topographic Analysis Kit (TAK) [41] of Topotoolbox [42] and ChiProfiler [43], combined with field evidence, 30 m ASTER global digital elevation model data were used for quantitative geomorphic analysis.

We extracted the changes of k_{sn} in this area to analyze the geomorphological features (Figure 4a). The spatial distribution of k_{sn} involved high values in the southern edge and low values in the northern edge of the Yabrai Shan. The highest k_{sn} value was identified at the southern edge, and high values were concentrated near the Yabrai range-front fault. The χ values were calculated to assess the migration trends of watersheds and to describe the mutual capture relationships among the rivers (Figure 4b). The water outlet was prescribed the same elevation and there were differences on both sides of watersheds. The χ values were higher in the northeastern segment, and gradually increased towards the northwest in the southwest and middle segments.

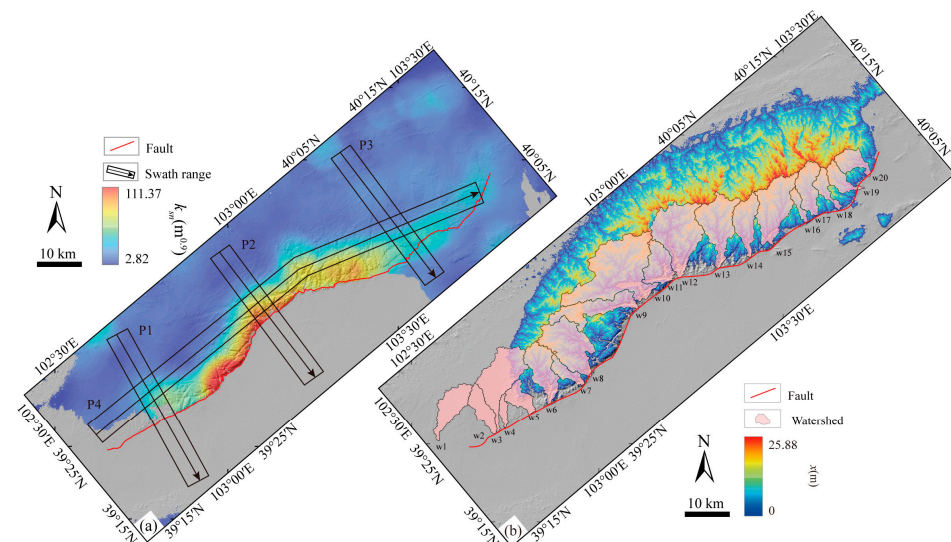


Figure 4. Distribution of geomorphic parameters in Yabrai Shan. (a) Channel steepness index and (b) χ . The black boxes in (a) indicate the swath profiles positions. The pink areas in (b) represent the watersheds used for the river longitudinal profiles.

Four swath profiles with widths of 5 km were extracted. One was parallel to the mountain range, whereas the remaining three were perpendicular (Figure 5). These swath profiles measured the maximum, minimum and average elevations in the strip area, and provided quantitative evidence on the elevation changes of peaks and valleys and the degree of erosion. In the southwestern segment of the Yabrai Shan, the average elevation is ~1400 m, the peak elevation is ~1800 m and the higher terrain is near the southern margin (Figure 5a). In the middle segment, the average elevation is ~1500 m, the maximum elevation difference reaches 450 m and the terrain fluctuates greatly, with the tilting degree being greater than that in the southwest segment (Figure 5b). In the northeastern segment, the average elevation is ~1700 m and the terrain is practically symmetrical (Figure 5c). Results show that the terrain in the northeastern section of Yabrai Shan is higher than that in the southwest section (Figure 5d).

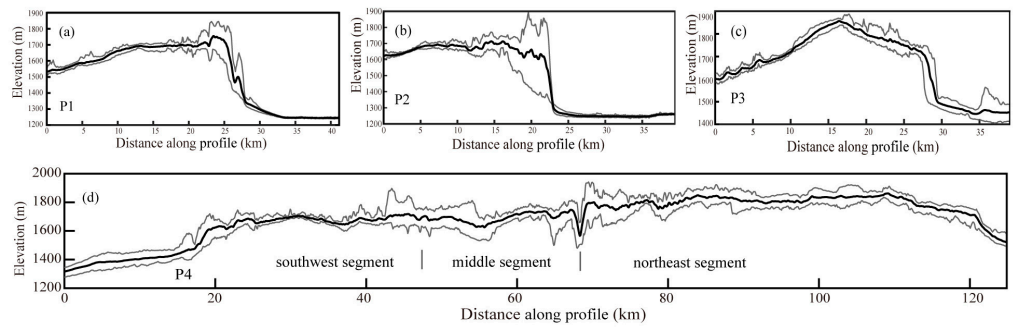


Figure 5. Swath profiles (a) in the southwest, (b) middle and (c) northeast of Yabrai Shan, and (d) along the strike of the Yabrai range-front fault. The location of these swath profiles was shown in Figure 4a. Bold black, and upper and lower lines in the strip area denote the average, maximum and minimum elevations, respectively. The maximum, minimum and average elevations in the strip area demonstrate the topographic features of the peaks, river valleys and average altitudes, respectively.

We also calculated the *HI* of basins with more than 10 km², while basins exceeding 100 km² were divided into sub-basins. For statistical analysis, 0.05 was used as a statistical unit of *HI* (Figure 6). The convex, S, and concave shapes corresponded to the infant (*HI* > 0.6), mature (0.35 < *HI* < 0.6) and old (*HI* < 0.35) stages of the geomorphological evolution [38]. The *HI* values of the basins ranged from 0.23 to 0.81 in the study area and were concentrated between 0.35 and 0.60 (71.8%). There were no *HI* values lower than 0.25 or higher than 0.80, with the 0.45~0.50 values accounting for the largest proportion (23.3%).

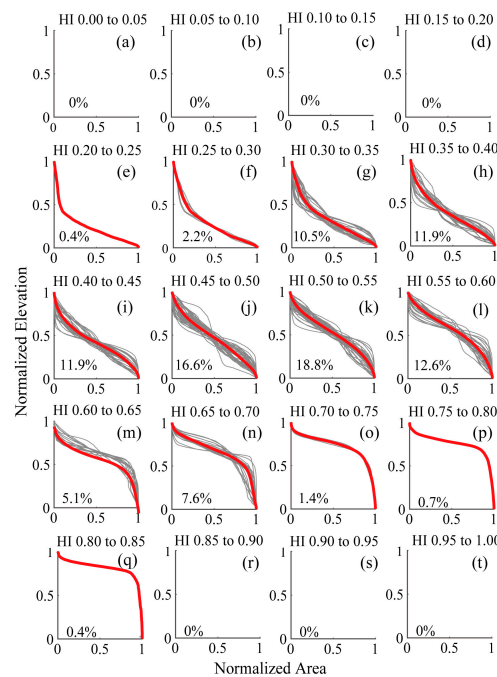


Figure 6. The *HI* values of basins. (a–t) represent the statistics of *HI*, 0.05 was used as a statistical unit. The gray lines are the *HI* curves of the basins and the red lines indicate the mean values.

The spatial distribution showed that the *HI* values in the southwestern Yabrai Shan were higher than those in the northeast section (Figure 7). The *HI* values near the fault were higher than those away from the fault. Moreover, along the Yabrai range-front fault, the *HI* values in the middle and southwest sections were higher than those in the northeast section.

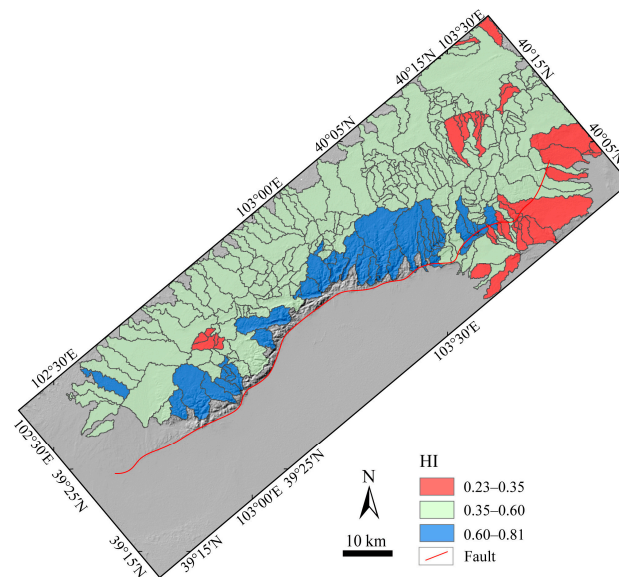


Figure 7. The *HI* values of the Yabrai Shan basins based on digital elevation model data.

During our field investigation, we had the opportunity to qualitatively observe the major river channels in this region (Figure 8). Channels are typically confined by bedrock walls, and bedrocks are severely ruptured and jointed, while plucking is the main erosion process.



Figure 8. (a–d) Photographs of the bedrock channel morphology in Yabrai Shan. The blue lines in (a), white dashed in (b) and white circle in (c) show the river direction, fault surface and a close view of a channel, respectively. The red arrows indicate the fault.

Twenty watersheds of Yabrai Shan were selected, and thirty-six rivers were subjected to channel longitudinal profile analysis. Eventually, knickpoints were identified along the river channels (Figure 9, Table 1).

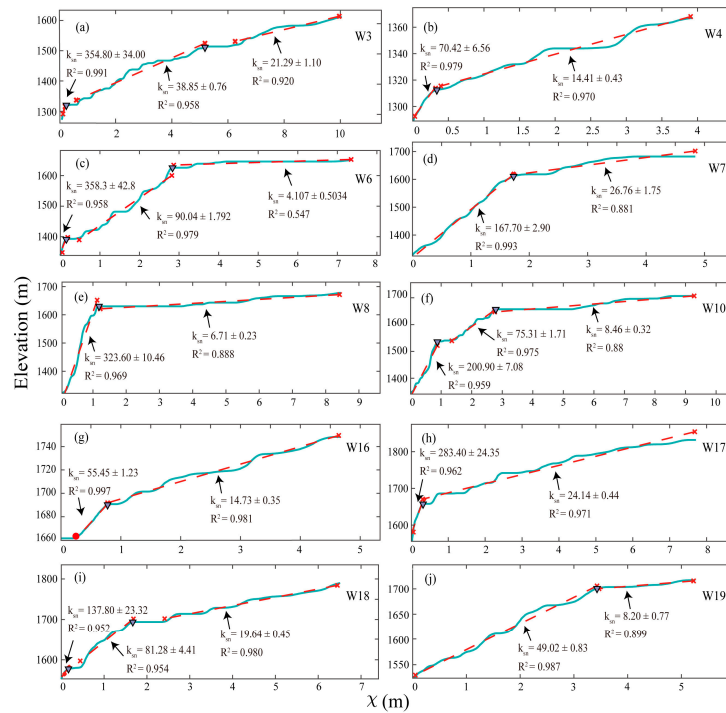


Figure 9. Longitudinal profile analysis of river channels. The selected watersheds were shown in Figure 4b. (a–j) represent streams. Watershed numbers are at the top right. Blue lines, red-dashed lines and red crosses indicate the original χ -z profiles, regressed χ -z profiles and the starts and ends of the fittings, respectively. Inverted triangles indicate abrupt changes of k_{sn} between upper and down reaches, recognized as knickpoints. The red dot is the fault through the river channel, as shown in (g).

Table 1. Results of river longitudinal profiles.

W No.	Das (km)	O-E (m)	Downstream		Upper Stream		Knickpoints				
			K_{Sn} ($m^{0.9}$)	R^2	K_{Sn} ($m^{0.9}$)	R^2	Kp-E (m)	Chi (χ)	A (km^2)	Dfm (km)	Dfd (km)
3	14.15	1268	354.75	0.99	38.85	0.96	1315	0.17	96.54	0.66	27.87
4	15.82	1289	70.42	0.98	14.41	0.97	1313	0.35	11.23	0.52	9.69
6	27.86	1339	358.35	0.96	90.04	0.98	1393	0.15	6.42	0.49	19.01
7	37.33	1329	167.66	0.99	26.76	0.88	1612	1.78	15.17	3.23	7.52
8	40.07	1322	323.60	0.97	6.70	0.89	1630	1.16	62.33	4.42	19.86
10	61.99	1341	200.91	0.96	75.31	0.97	1532	0.92	170.80	4.95	28.48
16	104.69	1659	55.45	1.00	14.73	0.98	1689	0.81	12.38	1.27	9.32
17	107.67	1556	283.43	0.96	24.14	0.97	1658	0.33	47.79	0.95	15.88
18	113.03	1554	137.85	0.95	81.28	0.95	1579	0.17	21.62	0.35	13.50
19	120.63	1524	49.02	0.99	8.19	0.90	1704	3.53	5.79	6.24	6.24

W No., Das, O-E, Kp-E, A, dfm, dfd are the watershed number. (Distance along the strike, Outlet Elevation, Knickpoint Elevation, Drainage Area, Distance From Mouth and Distance From Divide).

The integral approach was used to analyze the channel profiles with a reference concavity of 0.45. The lower reach had a high steepness index of $\sim 183 m^{0.9}$ in the southwestern Yabrai Shan, $\sim 259 m^{0.9}$ in the middle Yabrai Shan and $\sim 155 m^{0.9}$ in the northeastern Yabrai Shan. The middle reaches had lower steepness index values of $\sim 36 m^{0.9}$ in the southwestern Yabrai Shan, $\sim 55 m^{0.9}$ in the middle Yabrai Shan and $\sim 31 m^{0.9}$ in the northeastern Yabrai Shan. The upper reaches had low steepness index values of $\sim 23 m^{0.9}$ in the southwestern Yabrai Shan, $\sim 31 m^{0.9}$ in the middle Yabrai Shan and $\sim 17 m^{0.9}$ in the northeastern Yabrai Shan. The average elevation of the knickpoints was approximately $\sim 1507 m$ between the lower and middle reaches and approximately $\sim 1568 m$ between the middle and upper reaches.

5. Discussion

5.1. Coupling Relationship of Terrain-Geomorphologic Parameters-Tectonic Activities

Geomorphology is the result of internal and external forces, such as tectonic activities and climate change. Geomorphologic parameters are the quantitative expression of external morphology formed by the internal forces, recording the information of geomorphic evolution [21–23,34,44]. Compared with traditional topographic profiles, swath profiles can reflect the features of topographic fluctuation, thereby indicating the trend of macrotopography in the strip area [45]. In the middle segment, the maximum elevation difference, up to 500 m, may indicate the intense tectonic activity of a normal fault. In the northeast segment, the lower elevation difference is consistent with the previous research on the property of thrust and strike-slip fault [12]. The terrains manifest the different growth patterns in Yabrai Shan. In the southwestern and middle segments, the terrains incline towards the northwest, indicative of a typical normal fault-controlled landform (Figure 5a,b), and those in the northeastern section are relatively symmetric, demonstrating a range development in a state of natural expansion (Figure 5c). The overall characteristics of those are steep in the southeast and gentle in the northwest.

The spatial distribution of k_{sn} is influenced by the tectonic and non-tectonic factors, such as lithology, precipitation and tectonic activities [34]. Herein, these factors were all discussed. The strength of rock erosion resistance affects the erosion efficiency, thereby affecting the shape of the river channel [29]. Magmatic rocks were widely developed in the study area. Diorite has the largest distribution, and granite is also widely distributed. Gabbro is less distributed in the later plutons. According to the field investigation, many river channels involve a single lithology, like watershed 8 (Figure 10), and knickpoints were developed. Meanwhile, different types of bedrocks exhibited similar k_{sn} values. For example, the granites were widespread in the southwestern, middle and northeastern Yabrai Shan, and there were also little differences in k_{sn} . Hence, lithology was not the primary factor affecting the distribution of k_{sn} .

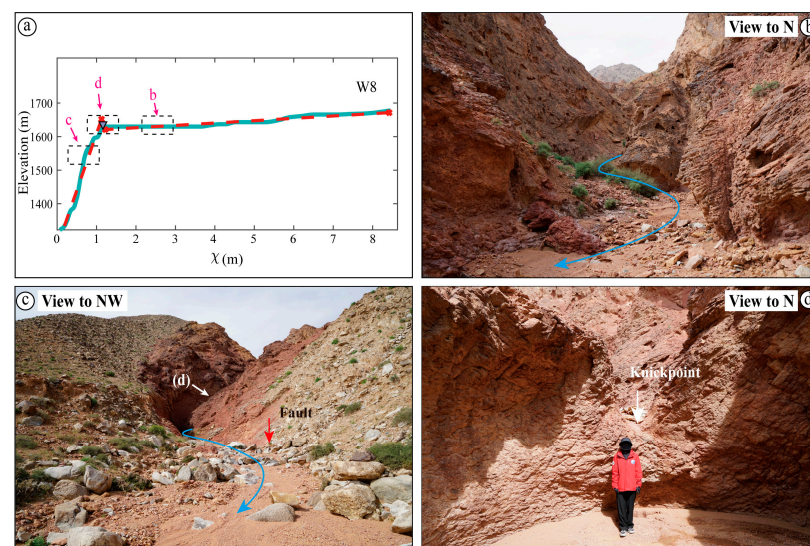


Figure 10. River longitudinal profile and field photographs of watershed 8. (a) Channel longitudinal profiles of watershed 8. Photographs of the river channel in the (b) upper reach, (c) down reach and (d) knickpoint. The black boxes and purple fonts in (a) indicate the locations in the river channel where the photographs (b–d) were taken. The blue lines in (b,c) show the river direction. The red and white arrows in (c) and white arrow in (d) indicate the fault, the location where the photograph (d) was taken and the knickpoint, respectively.

Increased precipitation results in increased river runoff, and therefore an enhanced erosion ability of the river, i.e., the erosion coefficient K increases, while k_{sn} decreases. As shown in Figure 11b, there were minor differences in precipitation across Yabrai Shan. The

average annual precipitation of the watersheds is less than 125 mm/yr, and the regional climate is dry. The spatial difference of geomorphic characteristics is independent of precipitation; therefore, precipitation is also not the primary cause.

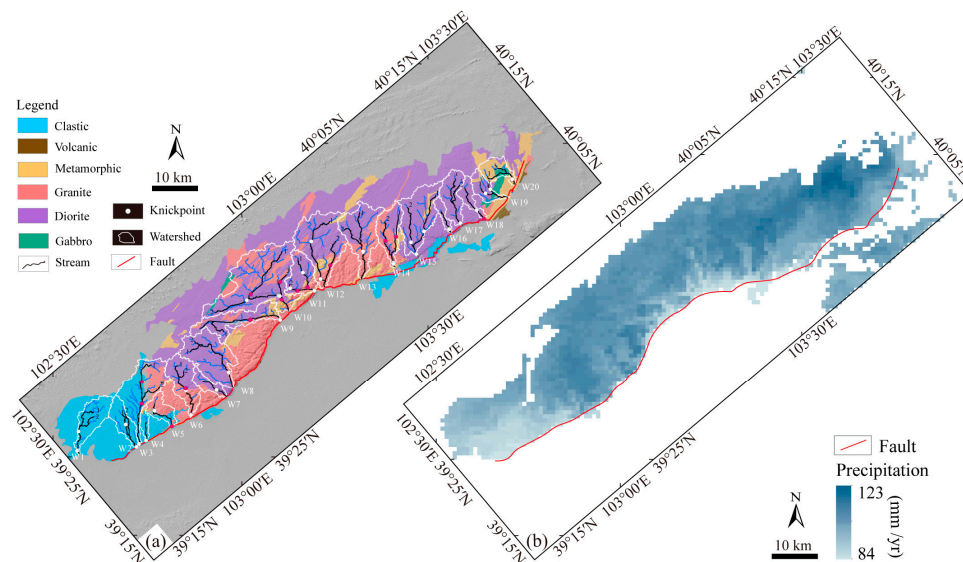


Figure 11. Lithology and precipitation maps of Yabrai Shan. (a) Distribution of the lithology, watersheds (W), streams and knickpoints. (b) Regional precipitation of Yabrai Shan. The white, blue, black and red lines represent the watershed, streams, streams used in the river longitudinal profile analysis and the Yabrai range-front fault, respectively. The red points in (a) were the knickpoints on the lithological boundary. Precipitation data derived from <http://www.worldclim.org/> (15 November 2021).

Studies on tectonic geomorphology have proven that regional tectonic activities, to a large extent, can be constrained by the normalized steepness index; hence, the distribution of k_{sn} largely depicts the intensity of tectonic activities [20,32,34,46]. The river channel steepness index suggested the uplift rate and was proportional to that of the bedrock. Tectonic activities in the southern margin of Yabrai Shan are strong and gradually decrease towards the north, while the southwestern and middle segments are stronger than the northeast segment. Meanwhile, the hypsometric integral of a drainage basin is a morphometric parameter for describing the basin geomorphology, represents the volume of materials that have not been eroded in the watershed [38] and is related to the effects of tectonic elements [39,40]. A high HI value indicates that most materials in the watershed have not been eroded, and the landform is in its infancy. According to the statistics, there were no HI values lower than 0.23 or higher than 0.81; values of $HI < 0.35$ were approximately 4% of the total, values of $0.35 < HI < 0.6$ were approximately 87% of the total and values of $HI > 0.6$ were approximately 9% of the total (Figure 6), revealing that Yabrai Shan is in the mature stage with strong tectonic activities. In summary, the spatial distribution of k_{sn} is decoupled from lithology and precipitation and coupled with tectonic activities. Previous research [12,14] on active tectonics also indicated that the geomorphological patterns are controlled by the tectonic activities of the Yabrai range-front fault.

5.2. The Implication of Knickpoints

The sudden increases of k_{sn} in the χ -plot profiles reflected increases in the fluvial incision rate, thereby developing knickpoints, with the underlying cause being the decline of the base level of erosion [29,34,47]. The development of knickpoints were subjected to the difference of rock erosion resistance. Knickpoints caused by lithology differences have no tectonic significance [34]. The comparison of the lithological map with the locations of knickpoints showed that fifteen knickpoints lie in the lithologic boundary. These knickpoints were generated by lithological differences and were not involved in the analysis of the geomorphic response time. Due to the coupling relationship between k_{sn} and tec-

tonic activities in this area [21,22,48], the variations of k_{sn} and the spatial distribution of knickpoints indicates that there were at least two tectonic acceleration events (Figure 12).

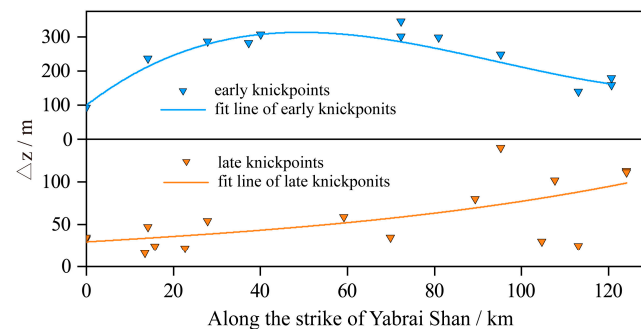


Figure 12. Scatter point distribution map of knickpoints in Yabrai Shan. Δz indicates the elevation difference between knickpoints and the watershed outlet. The blue points represent the early knickpoints and the orange points represent the late knickpoints. The line represents the fitting of the elevation difference between the knickpoints and the outlet.

Two stages of river incision were also found in the field, as shown in the photographs of the bedrock channel in watershed 10 (Figure 13). With the tectonic activity, the mountain was uplifted and the incision rate increased, thereby controlling and affecting the regional landform evolution [47]. Hence, the generation of knickpoints resulted from the adjustment responses of regional tectonic activities. In the early stage, the knickpoints migrated faster or occurred earlier in the middle segment of Yabrai Shan, manifesting the developmental features of normal faults. However, in the late stage, the migration speeds of knickpoints in the northeastern section of Yabrai Shan were higher than those in the southwestern and middle sections. The difference may have been induced by the change in tectonic stress.

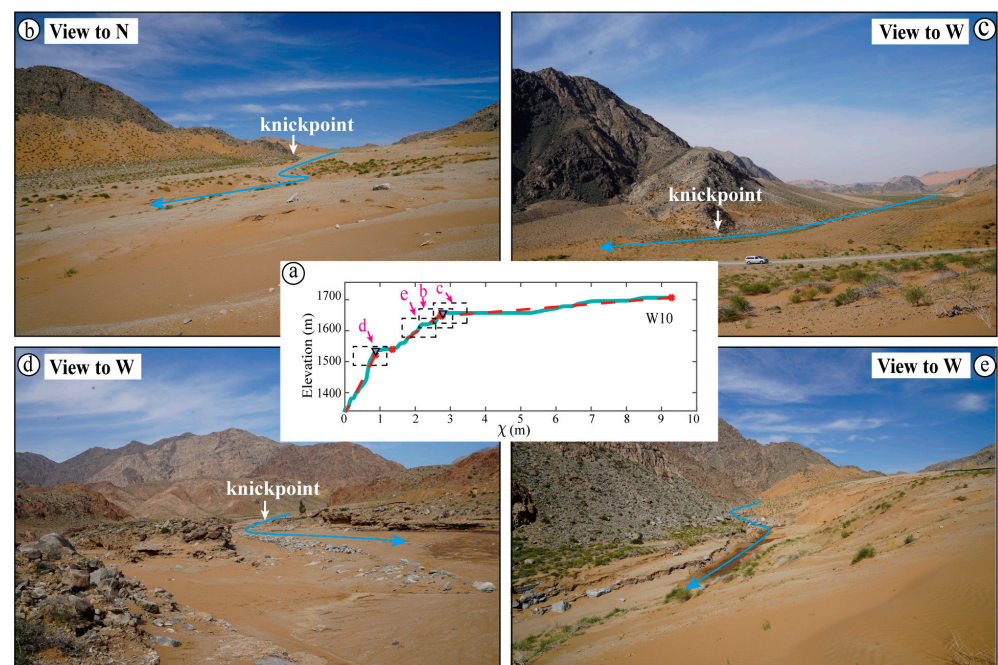


Figure 13. River longitudinal profile and field photographs of watershed 10. (a) Channel longitudinal profiles of watershed 10. Photographs of the river channel in the (b) knickpoint between the middle and upper reach, (c) upper reach and (d) knickpoint between the lower and middle reach. The black boxes and purple fonts in (a) represent the locations in the river channel where the photographs in (b–e) were taken. The blue lines and white arrows in (b–e) indicate the river direction and the knickpoints, respectively.

5.3. Geomorphic Response Time

Based on geomorphic displacement measurements and cosmogenic nuclide dating, Yu et al. obtained the average vertical fault slip rate [12]. In this study, we obtained geomorphic parameters, such as the relative elevation of knickpoints from the water outlet, k_{sn1} , k_{sn2} . By combining our results with previous studies on active faults in this area, the geomorphic response times of two tectonic acceleration events were estimated at 0.15–1.10 and 1.42–2.92 Ma (Figure 14), revealing a two-phase uplift of Yabrai Shan during the Late Cenozoic.

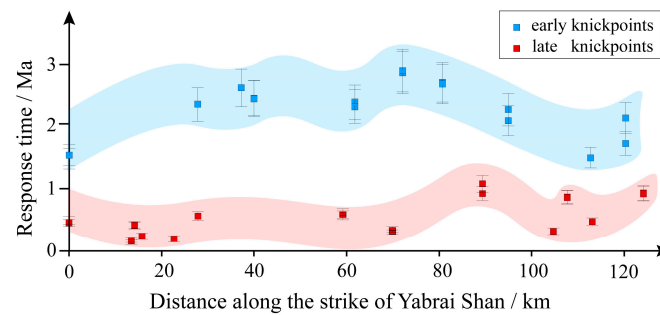


Figure 14. Geomorphic response times of the two-phase knickpoints in Yabrai Shan. The blue and red points indicate the early and late knickpoints, respectively.

The χ values indicated the stability of the drainage divide and reflected the dynamic changes of the current watershed. When a river network reaches equilibrium, the χ values are symmetrically distributed along the drainage divide [28,33,49]. The distribution of the χ values in Yabrai Shan demonstrated that the watersheds have not reached the steady state, the drainage divide moved to the northeast and the drainage area of the southeast basins will increase. Hence, the estimated response time was longer than the real response time, while the upper bound of the response time is reliable.

In the early stage, previous research indicated the Yabrai Shan was controlled by regional tensional stress in the NW-SE direction, and a normal fault with NE-SW strike and SE inclination was formed along the piedmont [12]. Controlled by this fault, the fault activity accelerated, and the mountain uplifted, thereby forming early knickpoints on the river channels. The geomorphic response times of the early knickpoints were ~1.42–2.92 Ma. The spatiotemporal distribution of these knickpoints showed that the middle segment of the Yabrai Shan responded to fault activity earlier than the southwestern and northeastern segments (Figure 14).

Contrary to the early knickpoints, the late knickpoints indicated that the uplift rate in the southwestern Yabrai Shan significantly decreased. Previous studies suggested that the southern Alashan Block was subjected to regional compressive stress in the NE-SW direction and the latest fault activity in the Alashan Block may be the latest impact of the north-eastern expansion of the Tibetan Plateau [10,50–52]. Hence, during the Late Cenozoic, the Yabrai range-front fault, under the influence of the northeastern expansion of the Tibetan Plateau, was transformed into a regional compressive environment, thereby affecting the fault activities, with the geomorphic response time being ~0.15–1.10 Ma (Figure 14).

Since the Cenozoic, the Tibetan Plateau has been experiencing a stepwise uplift and expansion to the northeast, exerting influence on the regional tectonic evolution [12,50–56]. According to apatite (U-Th)/He dating, the North Qilian Shan was rapidly uplifted at about 10 Ma [52]. Based on thermal analysis of the basin history, the Yumu Shan began to rise at 4.0 Ma [55]. Research on the active tectonics at the southern margin of Heli Shan revealed that the mountain uplift time was 1–3 Ma [6]. Due to the constraints of quantitative geomorphology, the NE expansion of Tibet Plateau entered the Hexi Corridor and Heli Shan at 0.6–2.1 Ma [50]. The tilting of Helan Shan shifted from the southwest to the northwest in response to the northeast expansion of the Tibetan Plateau at 0.1–1.4 Ma [51].

These studies indicate that the northeast expansion of the Tibetan Plateau is a continuous process, extending from the North Qilian Shan to the northeast towards Yumu

Shan, Heli Shan, Yabulai Shan and Helan Shan. Hence, the late stage knickpoints may be the result of the Tibetan Plateau extending northeast across the Hexi Corridor into the Alashan Block, causing rapid mountain uplift at 0.15–1.10 Ma. Consequently, the Yabrai Shan experienced the transformation from the original extensional environment, affected by the Ordos Block, to the compressional environment, affected by the NE expansion of the Tibetan Plateau after 1 Ma.

6. Conclusions

In this study, we conducted the quantitative geomorphological analysis and field investigation of Yabrai Shan, obtained the spatiotemporal distribution characteristics of the geomorphological parameters and studied the geomorphic evolution in this area. The conclusions are as follows:

- (1) The spatiotemporal distribution of geomorphic parameters is coupled with tectonic activity, and the geomorphic evolution of Yabulai Shan is controlled by that. The k_{sn} values indicate that the tectonic activity in the southern margin was strong, while gradually decreasing towards the north. In addition, the HI values reveal that the Yabrai Shan is in the mature stage of geomorphological evolution.
- (2) The variations of k_{sn} and the distribution of knickpoints indicate that there were at least two tectonic acceleration events. The characteristic distribution of the two-stage knickpoints is due to the altered tectonic stress in the area.
- (3) The geomorphic of Yabrai Shan evolution recorded the transformation in this area from the original extensional environment, affected by the Ordos Block, to the compressional environment, affected by the north-eastern expansion of the Tibetan Plateau after 1 Ma.

Author Contributions: T.J.: Conceptualization, Methodology, Investigation, Data curation, Visualization, Writing—original draft, Writing—review & editing; W.Z.: Conceptualization, Supervision, Funding acquisition, Methodology, Resources, Writing—review & editing; J.Y.: Methodology, Data curation, Resources, Writing—review & editing; D.Z.: Supervision, Conceptualization, Resources, Writing—review & editing; S.L. and Y.L.: Resources, Writing—review & editing; T.L., H.Z. and C.F.: Writing—review & editing. All authors have read and agreed to the published version of the manuscript.

Funding: This research was funded by the National Key Research and Development Program of China, grant number 2017YFC1500100, the Second Tibetan Plateau Scientific Expedition and Research Program (STEP), grant number 2019QZKK0901, the National Science Foundation of China, grant number 42174062 and 41774049, and the Guangdong Province Introduced Innovative R&D Team of Geological Processes and Natural Disasters around the South China Sea, grant number 2016ZT06N331.

Data Availability Statement: The ASTER DEM data used in this study are downloaded from the National Aeronautics and Space Administration (NASA) through the Earth data website <https://search.earthdata.nasa.gov/search> (15 November 2021). The Topotoolbox and ChiProfiler used in this study are downloaded through the GitHub website <https://github.com> (15 November 2021). Precipitation data derived from <http://www.worldclim.org/> (15 November 2021).

Acknowledgments: The authors thank all those who have contributed to this research. Special thanks to Bingxu Liu, Qing Tang, Zhikang Gong, Hui Peng and Yu Zhu for assisting us.

Conflicts of Interest: The authors declare no conflict of interest.

References

1. Burchfiel, B.C.; Deng, Q.D.; Molnar, P.; Royden, L.; Wang, Y.P.; Zhang, P.Z. Intracrustal detachment within zones of continental deformation. *Geology* **1989**, *17*, 748. [[CrossRef](#)]
2. Darby, B.; Ritts, B.; Yue, Y.; Meng, Q. Did the Altyn Tagh fault extend beyond the Tibetan Plateau. *Earth Planet. Sci. Lett.* **2005**, *240*, 425–435. [[CrossRef](#)]
3. Tapponnier, P. Oblique stepwise rise and growth of the Tibetan Plateau. *Science* **2001**, *294*, 1671–1677. [[CrossRef](#)] [[PubMed](#)]

4. Melissa, A.L.A.; Andrew, D.H.B.; Stephan, A.G.A.; Gombosuren, B.C.; Laura, E.W.D. Left-lateral sense offset of Upper Proterozoic to Paleozoic features across the Gobi Onon, Tost, and Zuunbayan faults in southern Mongolia and implications for other central Asian faults. *Earth Planet. Sci. Lett.* **1999**, *173*, 183–194.
5. Vincent, S.J.; Allen, M.B. Evolution of the Minle and Chaoshui Basins, China: Implications for Mesozoic strike-slip basin formation in Central Asia. *Geol. Soc. Am. Bull.* **1999**, *111*, 725–742. [[CrossRef](#)]
6. Zheng, W.J.; Zhang, P.Z.; He, W.G.; Yuan, D.Y.; Shao, Y.X.; Zheng, D.W.; Ge, W.P.; Min, W. Transformation of displacement between strike-slip and crustal shortening in the northern margin of the Tibetan Plateau: Evidence from decadal GPS measurements and late Quaternary slip rates on faults. *Tectonophysics* **2013**, *584*, 267–280. [[CrossRef](#)]
7. Zheng, W.J.; Zhang, H.P.; Zhang, P.Z.; Molnar, P.; Liu, X.W.; Yuan, D.Y. Late Quaternary slip rates of the thrust faults in western Hexi Corridor (Northern Qilian Shan, China) and their implications for northeastward growth of the Tibetan Plateau. *Geosphere* **2013**, *9*, 342–354.
8. Zheng, W.J.; Zhang, P.Z.; Ge, W.P.; Molnar, P.; Zhang, H.P.; Yuan, D.Y.; Liu, J.H. Late Quaternary slip rate of the South Heli Shan Fault (northern Hexi Corridor, NW China) and its implications for northeastward growth of the Tibetan Plateau. *Tectonics* **2013**, *32*, 271–293. [[CrossRef](#)]
9. Zheng, W.J. Geometric Pattern and Active Tectonics of the Hexi Corridor and Its Adjacent Regions. *Recent Dev. World Seismol.* **2010**, *3*, 33–36. [[CrossRef](#)]
10. Zheng, W.J.; Zhang, B.X.; Yuan, D.Y.; Chen, G.; Zhang, Y.P.; Yu, J.X.; Zhang, D.L.; Bi, H.Y.; Liu, B.X.; Yang, Y.J. Tectonic Activity in the Southern Alashan Block and the Latest Boundary of Outward Expansion on the Northeastern Tibetan Plateau, China. *J. Earth Sci. Environ.* **2021**, *43*, 224–236.
11. Yu, J.X. *Late Quaternary Slip Rates and Paleoearthquakes along the Yabrai Range-Front Fault in the Southern Gobi-Alashan Block*; Institute of Geology, China Earthquake Administration: Beijing, China, 2013. [[CrossRef](#)]
12. Yu, J.X. *Active Tectonics in the Southern Gobi-Alashan Block and its Response to the Interactions of the Adjacent Crustal Blocks*; Institute of Geology, China Earthquake Administration: Beijing, China, 2016. [[CrossRef](#)]
13. Ye, K.; Zhang, L.; Wang, T.; Shi, X.J.; Zhang, J.J.; Liu, C. Geochronology, geochemistry and zircon Hf isotope of the Permian intermediate acid igneous rocks from the Yabrai Mountain in western Alxa, Inner Mongolia, and their tectonic implications. *Acta Petrol. ET Mineral.* **2016**, *35*, 901–928.
14. Jin, F.X. *The Study of Quaternary Stratigraphic Sequence in Yabrai Mountain of Alxa, Inner Mongolian Autonomous Region*; China University of Geosciences: Beijing, China, 2014.
15. Du, J.X. *Role of Tectonic Uplift and Expansion within and Outside the Northeastern Tibetan Plateau in the Formation and Evolution of River and Desert Landscapes*; University of Chinese Academy of Sciences (Aerospace Information Research Institute): Beijing, China, 2021. [[CrossRef](#)]
16. Goren, L.; Fox, M.; Willett, S.D. Tectonics from fluvial topography using formal linear inversion: Theory and applications to the Inyo Mountains, California. *J. Geophys. Res. Earth Surf.* **2014**, *119*, 1651–1681. [[CrossRef](#)]
17. Kerby, A.D.H. Channel changes in badlands. *Geol. Soc. Am. Bull.* **1983**, *94*, 739–752.
18. Snyder, N.P.; Whipple, K.X.; Tucker, G.E.; Merritts, D.J. Landscape response to tectonic forcing: Digital elevation model analysis of stream profiles in the Mendocino triple junction region, northern California. *Geol. Soc. Am. Bull.* **2000**, *112*, 1250–1263. [[CrossRef](#)]
19. Cameron, W. Tectonics from topography: Procedures, promise, and pitfalls. *Tecton. Clim. Landsc. Evol.* **2006**, *398*, 55–74.
20. Pritchard, D.; Roberts, G.G.; White, N.J.; Richardson, C.N. Uplift histories from river profiles. *Geophys. Res. Lett.* **2009**, *36*, L24301. [[CrossRef](#)]
21. Kirby, E.; Whipple, K.X.; Tang, W.; Chen, Z. Distribution of active rock uplift along the eastern margin of the Tibetan Plateau: Inferences from bedrock channel longitudinal profiles. *J. Geophys. Res.* **2003**, *108*, 2217. [[CrossRef](#)]
22. Hu, X.F.; Pan, B.T.; Kirby, E.; Li, Q.Y.; Geng, H.P.; Chen, J.F. Spatial differences in rock uplift rates inferred from channel steepness indices along the northern flank of the Qilian Mountain, northeast Tibetan Plateau. *Chin. Sci. Bull.* **2010**, *55*, 3205–3214. [[CrossRef](#)]
23. Fox, M.; Bodin, T.; Shuster, D.L. Abrupt changes in the rate of Andean Plateau uplift from reversible jump Markov Chain Monte Carlo inversion of river profiles. *Geomorphology* **2015**, *238*, 1–14. [[CrossRef](#)]
24. Wu, M.B.; Liu, C.Y.; Zheng, M.L.; Yun, J.B. Jurassic depositional-tectonic evolution in the Yabrai basin, western Inner Mongolia, China and direction of petroleum exploration. *Geol. Bull. China* **2007**, *26*, 857–863.
25. Zhong, F.P.; Zhong, J.H.; You, W.F.; Wang, Y.; Zhang, L.; Bian, Q.; Abdul, R.; Man, A.T.; Gao, Y.F.; Wang, J.H. Study on Sedimentary Facies and Environment of Middle Jurassic in Hongliugou of Yabrai Basin Inner Mongolia. *Geol. Bull. China* **2010**, *32*, 149–154.
26. *Regional Geology of Gansu Province*; Geological Publishing House: Beijing, China, 1989.
27. Hack, J. *Studies of Longitudinal Stream Profiles in Virginia and Maryland*; USGS Professional Paper: Washington, DC, USA, 1957; Volume 294, pp. 45–97.
28. Howard, A.D. A detachment-limited model of drainage basin evolution. *Water Resour. Res.* **1994**, *30*, 2261–2285. [[CrossRef](#)]
29. Whipple, K.X.; Tucker, G.E. Dynamics of the stream-power river incision model: Implications for height limits of mountain ranges, landscape response timescales, and research needs. *J. Geophys. Res. Solid Earth* **1999**, *104*, 17661–17674. [[CrossRef](#)]
30. Kirby, E.; Whipple, K.X. Quantifying differential rock-uplift rates via stream profile analysis. *Geology* **2001**, *29*, 415–418. [[CrossRef](#)]
31. Perron, J.T.; Royden, L. An integral approach to bedrock river profile analysis. *Earth Surf. Proc. Land* **2012**, *38*, 570–576. [[CrossRef](#)]
32. Wang, Y.Z.; Zhang, H.P.; Zheng, D.W.; Yu, J.X.; Xiao, L. A brief introduction to the new method for river profile analysis: Integral Approach. *Seismol. Geol.* **2017**, *39*, 1111–11126.

33. Willett, S.D.; McCoy, S.D.; Perron, J.T.; Goren, L.; Chen, C.Y. Dynamic Reorganization of River Basins. *Science* **2014**, *343*, 1117. [[CrossRef](#)]
34. Kirby, E.; Whipple, K.X. Expression of active tectonics in erosional landscapes. *J. Struct. Geol.* **2012**, *44*, 54–75. [[CrossRef](#)]
35. Royden, L.; Perron, J.T. Solutions of the stream power equation and application to the evolution of river longitudinal profiles. *J. Geophys. Res. Earth* **2013**, *118*, 497–518. [[CrossRef](#)]
36. Fox, M.; Goren, L.; May, D.A.; Willett, S.D. Inversion of fluvial channels for paleorock uplift rates in Taiwan. *J. Geophys. Res.* **2014**, *119*, 1853–1875. [[CrossRef](#)]
37. Goren, L. A theoretical model for fluvial channel response time during time-dependent climatic and tectonic forcing and its inverse applications. *Geophys. Res. Lett.* **2016**, *43*, 10753–10763. [[CrossRef](#)]
38. Strahler, A.H. Hypsometric (Area-Altitude) Analysis of Erosional Topography. *Geol. Soc. Am. Bull.* **1952**, *63*, 1117–1142. [[CrossRef](#)]
39. Zhu, S.J.; Tang, G.A.; Li, F.Y.; Xiong, L.Y. Spatial variation of hypsometric integral in the Loess Plateau based on DEM. *Acta Geogr. Sin.* **2013**, *68*, 921–932.
40. Zhao, H.Z.; Li, Y.L.; Yang, J.C.; Lu, H.H. Influence of area and space dependence for hypsometric integral and its geological implications. *Geogr. Res.* **2010**, *29*, 271–282.
41. Forte, A.M.; Whipple, K.X. Short communication: The Topographic Analysis Kit (TAK) for TopoToolbox. *Earth Surf. Dyn.* **2019**, *7*, 87–95. [[CrossRef](#)]
42. Schwanghart, W.; Scherler, D. Short Communication: TopoToolbox 2—MATLAB-based software for topographic analysis and modeling in Earth surface sciences. *Earth Surf. Dyn.* **2014**, *2*, 1–7. [[CrossRef](#)]
43. Gallen, S.F.; Wegmann, K.W. River profile response to normal fault growth and linkage: An example from the Hellenic forearc of south-central Crete, Greece. *Earth Surf. Dyn.* **2017**, *5*, 161–186. [[CrossRef](#)]
44. Whipple, K.X.; Kirby, E.; Brocklehurst, S.H. Geomorphic limits to climate-induced increases in topographic relief. *Nature* **1999**, *401*, 39–43. [[CrossRef](#)]
45. Grohmann, C. Morphometric analysis in geographic information systems: Applications of free software GRASS and R. *Comput. Geosci.* **2004**, *30*, 1055–1067. [[CrossRef](#)]
46. Zhang, H.P.; Zhang, P.Z.; Fan, Q.C. Initiation and recession of the fluvial knickpoints: A case study from the Yalu River-Wangtian'e volcanic region, northeastern China. *Sci. China Earth Sci.* **2011**, *54*, 1746–1753. [[CrossRef](#)]
47. Willett, S.D.; Hovius, N.; Brandon, M.T.; Fisher, D. *Tectonics, Climate, and Landscape Evolution*; Special Paper of the Geological Society of America; Geological Society of America: Boulder, CO, USA, 2006. [[CrossRef](#)]
48. Wobus, C.W.; Crosby, B.T.; Whipple, K.X. Hanging valleys in fluvial systems: Controls on occurrence and implications for landscape evolution. *J. Geophys. Res.* **2016**, *111*, F02017. [[CrossRef](#)]
49. Whipple, K.X.; Forte, A.M.; DiBiase, R.A.; Gasparini, N.M.; Ouimet, W.B. Timescales of landscape response to divide migration and drainage capture: Implications for the role of divide mobility in landscape evolution. *J. Geophys. Res.* **2017**, *122*, 248–273. [[CrossRef](#)]
50. Yang, J.J.; Zheng, W.J.; Wang, Y.; Bi, H.Y.; Zhang, D.L.; Zhang, P.Z.; Chen, G.; Wang, W.T. Quantitative geomorphological constraints on the landform evolution of the current active boundary of the northeastern Tibetan Plateau. *Geomorphology* **2020**, *358*, 107–120. [[CrossRef](#)]
51. Li, Y.G.; Zheng, W.J.; Yang, J.J.; Zhang, D.L.; Zhou, H.Y.; Liu, T. Early Quaternary Tectonic Transformation of the Helan Shan: Constraints Due to Quantitative Geomorphology. *Front. Earth Sci.* **2022**, *10*, 825849. [[CrossRef](#)]
52. Zheng, D.W.; Clark, M.K.; Zhang, P.Z.; Zheng, W.J.; Farley, K.A. Erosion, fault initiation and topographic growth of the North Qilian Shan (northern Tibetan Plateau). *Geosphere* **2010**, *6*, 937–941. [[CrossRef](#)]
53. Deng, Q.; Zhang, P.; Ran, Y.; Yang, X.; Chu, Q. Basic characteristics of active tectonic of China (in Chinese). *Sci. China Ser. D Earth Sci.* **2003**, *46*, 357–372.
54. Zhang, P.; Shen, Z.; Wang, M.; Gan, W.; Burgmann, R.; Molnar, P. Continuous deformation of the Tibetan Plateau from global positioning system data. *Geology* **2004**, *32*, 809–812. [[CrossRef](#)]
55. Wang, Y.Z.; Zheng, D.W.; Pang, J.Z.; Zhang, H.P.; Wang, W.T.; Yu, J.X.; Zhang, Z.Q.; Zheng, W.J.; Zhang, P.Z.; Li, Y.J. Using slope-area and apatite fission track analysis to decipher the rock uplift pattern of the Yumu Shan: New insights into the growth of the NE Tibetan Plateau. *Geomorphology* **2018**, *308*, 118–128. [[CrossRef](#)]
56. Molnar, P.; England, P.; Martinrod, J. Mantle dynamics, uplift of the Tibetan Plateau, and the Indian Monsoon. *Rev. Geophys.* **1993**, *31*, 357–396. [[CrossRef](#)]